RSC Advances

PAPER

View Article Online
View Journal | View Issue

Cite this: *RSC Adv.*, 2025, **15**, 51209

Pyrazolyl-functionalised Ag(I)–NHC complexes: synthesis, characterisation, antibacterial activity, and computational investigation

Ngonidzashe Ruwizhi, [a] Karen Pillay, [b] Janade Moodley, [b] Thishana Singh, [a] Bernard Omondi [a] and Muhammad D. Bala [*a]

In this study, five pyrazolyl-functionalised azolium salts with varying N-substituents (R-group) on the (benz) imidazolium rings, *i.e.* 3-(2-(3,5-dimethyl-1*H*-pyrazol-1-yl) ethyl)-1-R-1*H*-imidazole-3-ium chloride, where R = methyl (**1a**), ethyl (**1b**), benzyl (**1c**) and 3-(2-(3,5-dimethyl-1*H*-pyrazol-1-yl)ethyl)-1-R-1*H*-benzo[*d*]imidazole-3-ium chloride, where R = methyl (**1d**), ethyl (**1e**) were synthesised. Corresponding silver(I)–N-heterocyclic carbene complexes **2a–e** were also synthesised from the deprotonation of the salts. All the compounds were characterised by spectroscopic and analytical techniques. In addition, all the salts and Ag(I) complexes were utilised as *in vitro* antibacterial agents against a broad spectrum of bacterial strains. Among the synthesised complexes, compound **2c** bearing a benzyl N-substituent demonstrated the highest potency with IC_{50} values and bacterial inhibition percentages comparable to the standard drug neomycin. Theoretical methods, including DFT calculations, were used to examine electronic effects and SWISSADME to predict enhanced activity for the benzimidazole-containing compounds as compared to those bearing simple imidazole. Also examined is the role of the *N*-benzyl moiety in enhancing the antibacterial activity of complex **2c**.

Received 31st July 2025
Accepted 12th December 2025

DOI: 10.1039/d5ra05570a

rsc.li/rsc-advances

1 Introduction

Antimicrobial resistance has emerged as a global health threat, and recent estimates indicate a growing trend in antibiotic resistance, with thousands of deaths reported annually.[1] Alarmingly, antimicrobial resistance appears to be spreading faster than the rate at which new, potent antibiotics are being introduced into clinical use. Alternative methods of combating the rapid drug resistance to microbes include structural modification and optimisation of existing antibiotics to improve the spectrum of activity while maintaining the safety and bioavailability profiles.[2] The lack of effective antibiotics can substantially compromise numerous medical procedures, including organ transplant surgery, the care of premature infants and the treatment of critically ill patients.[3] Since ancient times, metallodrugs have been widely used for therapy and diagnostics of a wide range of ailments.[4] Silver was historically used for its antibacterial properties until the discovery of antibiotics such as penicillin, which essentially replaced it in therapeutic applications.[5–7]

The use of silver has reemerged in recent years owing to the high bioavailability of the Ag(I) cation, which significantly contributes to its antimicrobial activity.[8] Apart from silver, several other metal-based antimicrobial agents have been reported to show promising efficacy against several microbes. A recent review reported some complexes based on manganese, cobalt, zinc, ruthenium, silver, iridium and platinum that exhibit good to excellent antibacterial activity against selected bacterial strains.[9] Recent studies reported cationic aggregation-induced emission active Ru(II) and Ir(III) complexes, with the most potent having antibacterial activity in the range of 1–9 μM against the selected Gram-positive strains.[10,11] Moreover, the emergence of antimicrobial resistance has led to a decline in the use of metallic silver and simple silver salts in a variety of medicinal applications.[12]

A key challenge is the loss of activity due to the uncontrolled loss/release of silver cations. Although the mechanism of action of silver cations is not completely established, researchers believe that the Ag(I) cation has a unique affinity for soft bases, such as thiol groups (R-SH), which are found in enzymes or proteins on the bacterial cell membrane. Reports suggest that Ag(I) cations disrupt the bacterial electron transport chain activity, potentially leading to the generation of reactive oxygen species and the depletion of antioxidants in bacterial cells.[13–16] Hence, reducing the uncontrolled release of Ag(I) ions through ligand design and the development of silver compounds with precisely controlled structural variations is necessary. Imidazole and benzimidazole derivatives have shown antimicrobial activity, and studies have shown that such compounds, when complexed to transition

[a]*School of Agriculture and Science, Discipline of Chemistry, University of KwaZulu-Natal, Westville Campus, Private Bag X54001, Durban 4000, South Africa*
[b]*School of Agriculture and Science, Discipline of Biological Sciences, University of KwaZulu-Natal, Westville Campus, Private Bag X54001, Durban 4000, South Africa. E-mail: bala@ukzn.ac.za*

metal centres (metallodrugs), often demonstrate superior antimicrobial potency than the free organic molecules.[9,17]

Recently, the N-heterocyclic carbene (NHC) ligands, which are five-membered heterocyclic azolium entities commonly based on imidazoles and triazoles, have garnered immense attention in various spheres of synthetic chemistry, including catalysis and biological applications.[2,13] This is due to their structural stability, variability and ease of synthesis in high yields, which is vital in controlling the stability and biological activity of their silver(I) complexes.[18] Additionally, research has shown that fusion with an aromatic benzene ring, such as in benzimidazoles, helps to further enhance the stability of the metal–carbene (M–C) bond.[19] Consequently, many benzimidazole-based Ag(I)–NHC complexes have been reported to be air- and water-stable, vital for applications in biological systems. Hence, they are more widely studied than Ag(I)–NHC complexes of simple imidazolylidene ligands.[20] The strong M–C bond allows for the slow release of the silver ions into the biological medium, increasing their residence time in the system and subsequent increase in efficacy.[21] In addition to the silver metal centre, structural modifications such as incorporating lipophilic groups on the NHC, such as alkyl chains, increase the lipophilicity of the Ag(I) complex, thus resulting in enhanced cell wall penetration.[22,23]

As an illustration of the range of activity of Ag(I)–NHC complexes, Bensalah *et al.* reported minimum inhibitory concentrations (MICs) as low as 10 mmol L^{-1} against *S. aureus* and 11 mmol L^{-1} against MRSA.[24] Meanwhile, Mnasri and coworkers reported complexes with antibacterial activities against a broad range of bacterial strains comparable to ampicillin.[25] Ghdhayeb *et al.* reported their complexes to show inhibition zones of 20 and 25 mm against *E. coli* and *S. aureus* at 100 and 200 μg mL^{-1}, respectively.[26] In addition, several pyrazole derivatives have also been reported to have antibacterial activity comparable to standard drugs.[27]

To complement experimental approaches, density functional theory (DFT), a widely used quantum-mechanical computational method, provides valuable insights into molecular geometry, electronic distribution, frontier molecular orbitals, and energetics.[28] In recent years, DFT has become an indispensable predictive tool used prior to experimental investigations, allowing researchers to model and optimise structures, assess reaction pathways, and evaluate key molecular properties such as binding energies, HOMO–LUMO gaps, and charge distribution.[29] These theoretical predictions not only guide experimental design but also serve to rationalise and validate experimental observations, thereby enhancing the reliability and efficiency of structure–activity relationship studies.[30] Herein, we report the utilisation of previously unreported imidazolium and benzimidazolium salts and their Ag(I)–NHC complexes as antibacterial agents using a combination of experimental and computational studies.

2 Experimental

2.1 Materials and methods

Reagent-grade acetylacetone, hydrazine hydrate, benzimidazole, 1-ethylimidazole and 1-methylimidazole were purchased from Merck. All reactions were carried out in a dry nitrogen atmosphere using standard Schlenk techniques. Thin-layer chromatography was done using TLC plates coated with silica gel. All solvents were distilled under nitrogen using the appropriate drying agent, stored in solvent reservoirs (containing 4 Å molecular sieves), and purged with nitrogen. ^{1}H- and ^{13}C-NMR were recorded using the 600 MHz Bruker Ultra Shield spectrometer. Chemical shifts for ^{1}H and ^{13}C spectra were recorded in ppm relative to the residual proton of $CDCl_3$ (^{1}H: δ 7.24; ^{13}C: δ 77.0) and DMSO-d_6 (^{1}H: δ 2.50; ^{13}C: δ 39.5) with tetramethylsilane as the internal standard. The elemental composition of the compounds was analysed using a CHN Thermo Scientific Flash 2000 Elemental Analyser. The FT-IR spectra were recorded using a PerkinElmer Attenuated Total Reflectance (ATR) spectrometer. UV-vis spectra were recorded with a PerkinElmer Lambda 365+ UV/vis spectrophotometer, and the compounds were dissolved in DMSO. Melting point analysis was performed on an MP-200D-HR Stuart high-resolution digital melting point apparatus.

2.2 Synthesis of ligand precursors

2.2.1 Synthesis of 3,5-dimethyl-1*H*-pyrazole. Hydrazine monohydrate (1.1 equiv.) in THF (2 mL $mmol^{-1}$) was added to a stirred solution of 2,4-pentanedione in THF (2 mL $mmol^{-1}$) over a period of 30 min *via* a syringe, and the reaction mixture was stirred overnight. The reaction mixture was concentrated *in vacuo* prior to adding water (50 mL). The desired product was extracted by DCM (3 × 50 mL), the combined organic extracts dried over anhydrous $MgSO_4$ and concentrated *in vacuo* to give 3,5-dimethyl-1*H*-pyrazole.[31]

2.2.2 Synthesis of 1-(2-chloroethyl)-3,5-dimethyl-1*H*-pyrazole. A 50 mL 1,2-dichloroethane solution of KOH (1.5 mol. equiv.), K_2CO_3 (1.5 mol. equiv.), tetrabutylammonium chloride (0.5 mol. equiv.), and 3,5-dimethylpyrazole (4.00 g, 0.04 mmol) was heated at 45 °C for 3.5 h. The solution was filtered, washed with water, and dried with anhydrous $MgSO_4$. The removal of the solvent under vacuum gave a yellow liquid as the pure product.[32]

2.2.3 Synthesis of 1-methylbenzimidazole and 1-ethylbenzimidazole. Benzimidazole (1 mol equiv.) and excess KOH in DMF for 15 minutes, after which 1.5 mol equiv. of the respective alkyl source (iodomethane and bromoethane for 1-methylbenzimidazole and 1-ethylbenzimidazole, respectively) was added and left to stir at room temperature for 3 hours. The work-up of 1-ethylimidazole, 1-methylbenzimidazole, and 1-ethylbenzimidazole involved diluting the reaction mixture with water to break the DMSO and DMF and neutralising the residual base. All organics were then extracted with DCM (30 mL × 5). The combined organic extracts were then washed with more water till neutral to litmus, then dried with anhydrous magnesium sulphate. All volatiles were then removed under reduced pressure to yield the required product.[33–36]

2.3 General procedure for the synthesis of salts 1a–e

A solvent-free mixture of 1-(2-chloroethyl)-3,5-dimethyl-1*H*-pyrazole and an appropriate N-substituted imidazole with a mole

ratio 1 : 1 was heated for approximately 18 hours. The temperature of the reaction depended on the type of N-substituted imidazole. After the reaction time, the crude product was washed several times with ethyl acetate to remove any residual starting materials.[32]

2.3.1 3-(2-(3,5-Dimethyl-1*H*-pyrazol-1-yl) ethyl)-1-methyl-1*H*-imidazole-3-ium chloride, (1a). Hygroscopic light brown oil. Yield 1.48 g, 90%. FT-IR: ν_{max}/cm^{-1} 1555 (CN). ^{1}H-NMR (600 MHz, DMSO-d_6) δ 8.86 (s, 1H), 7.65 (d, J = 1.8 Hz, 1H), 7.51 (d, J = 1.8 Hz, 1H), 5.80 (s, 1H), 4.56–4.51 (m, 2H), 4.36 (t, J = 5.9 Hz, 2H), 3.82 (s, 3H), 2.07–2.06 (d, 6H). ^{13}C-NMR (151 MHz, DMSO-d_6) δ 147.28, 139.91, 137.56, 123.95, 123.06, 105.48, 48.91, 47.68, 36.18, 13.75, 10.72. LRMS (ESI): m/z calcd for $[C_{11}H_{17}N_4]^+$: 205.1448; found: 205.1455. Anal. calcd for $C_{11}H_{17}ClN_4$ C, 54.88; H, 7.12; N, 23.27; found: C, 54.79; H, 7.03; N, 23.15.

2.3.2 3-(2-(3,5-Dimethyl-1*H*-pyrazol-1-yl)ethyl)-1-ethyl-1*H*-imidazole-3-ium chloride, (1b). Hygroscopic light brown oil. Yield 1.73 g, 93%. FT-IR: ν_{max}/cm^{-1} 1555 (CN). ^{1}H-NMR (600 MHz, DMSO-d_6) δ: 9.13 (s, 1H), 7.83 (d, J = 1.8 Hz, 1H), 7.64 (d, J = 1.8 Hz, 1H), 5.78 (s, 1H), 4.57 (d, J = 5.9 Hz, 2H), 4.39 (d, J = 5.9 Hz, 2H), 4.18 (q, J = 7.3 Hz, 2H), 2.05 (d, J = 12.5 Hz, 6H), 1.36 (t, J = 7.3 Hz, 3H). ^{13}C-NMR (151 MHz, DMSO-d_6) δ: 147.27, 139.88, 136.74, 123.16, 122.54, 105.42, 49.02, 47.70, 44.60, 15.81, 13.74, 10.67. LRMS (ESI): m/z calcd for $[C_{12}H_{19}N_4]^+$: 219.1605; found: 219.1755. Anal. calcd for $C_{11}H_{17}ClN_4$ C, 56.57; H, 7.52; N, 21.99, found: C, 56.48; H, 7.46; N, 21.85.

2.3.3 3-(2-(3,5-Dimethyl-1*H*-pyrazol-1-yl)ethyl)-1-benzyl-1*H*-imidazole-3-ium chloride, (1c). Compound **1c** was synthesised the same way as **1a**, except that the reaction temperature was raised between 100 and 110 °C. Hygroscopic off-white solid. Yield 1.64 g, 91%, mp 146–148 °C. FT-IR: ν_{max}/cm^{-1} 1457 (CN). ^{1}H-NMR (600 MHz, DMSO-d_6) δ: 9.01 (s, 1H), 7.86 (d, J = 1.8 Hz, 1H), 7.71 (d, J = 1.8 Hz, 2H), 7.44–7.33 (m, 5H), 5.73 (s, 1H), 5.44 (s, 2H), 4.57 (t, J = 5.7 Hz, 2H), 4.38 (t, J = 5.7 Hz, 2H), 1.91–2.04 (d, 6H). ^{13}C-NMR (151 MHz, DMSO-d_6) δ: 147.34, 139.81, 137.16, 135.40, 129.37, 129.13, 128.59, 123.57, 122.94, 105.41, 52.17, 49.23, 47.62, 13.75, 10.62. LRMS (ESI): m/z calcd for $[C_{17}H_{21}N_4]^+$: 281.1761, found: 281.1762. Anal. calcd for $C_{17}H_{24}ClN_4$: C, 64.45; H, 6.68; N, 17.68, found: C, 64.37; H, 6.53; N, 17.62.

2.3.4 3-(2-(3,5-Dimethyl-1*H*-pyrazol-1-yl)ethyl)-1-methyl-1*H*-benzo[*d*]imidazole-3-ium chloride, (1d). White hygroscopic solid. Yield 1.85 g, 93%, mp 156–158 °C. FT-IR: ν_{max}/cm^{-1} 1562 (CN). ^{1}H-NMR (600 MHz, DMSO-d_6) δ: ^{1}H-NMR (600 MHz, DMSO-d_6) δ: 9.74 (s, 1H), 8.01 (d, J = 8.3 Hz, 1H), 7.75 (d, J = 8.3 Hz, 1H), 7.67 (t, J = 7.7 Hz, 1H), 7.62 (t, J = 7.7 Hz, 1H), 5.72 (s, 1H), 4.90 (t, J = 5.7 Hz, 2H), 4.46 (t, J = 5.8 Hz, 2H), 4.09 (s, 3H), 2.02 (s, 3H), 1.94 (s, 3H). ^{13}C-NMR (151 MHz, DMSO-d_6) δ: 147.26, 143.71, 139.79, 131.96, 131.49, 126.92, 126.88, 113.91, 113.66, 105.62, 47.20, 46.93, 33.69, 13.56, 10.67. LRMS (ESI): m/z calcd for $[C_{15}H_{19}N_4]^+$: 255.1605; found: 255.1605. Anal. calcd for $C_{15}H_{19}ClN_4$: C, 61.96; H, 6.59; N, 19.27, found: C, 61.86; H, 6.44; N, 19.09.

2.3.5 3-(2-(3,5-Dimethyl-1*H*-pyrazol-1-yl)ethyl)-1-ethyl-1*H*-benzo[*d*]imidazole-3-ium chloride, (1e). White hygroscopic solid. Yield 1.77 g, 92%, mp 123–125 °C. FT-IR: ν_{max}/cm^{-1} 1563 (CN). ^{1}H-NMR (600 MHz, DMSO-d_6) δ ^{1}H NMR (600 MHz, DMSO-d_6) δ 9.41 (s, 1H), 8.02 (d, J = 8.2 Hz, 1H), 7.76 (d, J = 8.1 Hz, 1H), 7.66 (t, J = 7.7 Hz, 1H), 7.62 (t, J = 7.7 Hz, 1H), 5.71 (s, 1H), 4.84 (t, J = 5.7 Hz, 2H), 4.50–4.46 (m, 2H), 4.46–4.42 (m, 2H), 1.94 (s, 3H), 1.92 (s, 3H), 1.47 (t, J = 7.3 Hz, 3H). ^{13}C-NMR (151 MHz, DMSO-d_6) δ: 147.25, 142.97, 139.79, 131.59, 131.03, 126.95, 126.90, 113.96, 113.84, 105.56, 47.09, 46.97, 42.42, 14.85, 13.56, 10.64. LRMS (ESI): m/z calcd for $[C_{16}H_{21}N_4]^+$: 269.1761, found: 269.1758. Anal. calcd For $C_{16}H_{21}ClN_4$: C, 63.04; H, 6.94; N, 18.38, found: C, 62.94; H, 6.81; N, 18.24.

2.4 General procedure for the synthesis of the Ag(I)–NHC complexes

A solution of an azolium salt (1.0 mmol) (**1a–e**), Ag_2O (1.0 mmol) in dry dichloromethane (15 mL) was stirred for 48 hours at room temperature in the dark. After the reaction time, the reaction mixture was filtered through Celite, and the solvent was removed under vacuum. The crude products (**2a–e**) were recrystallised from dichloromethane/diethyl ether (1 : 3).[37] All the Ag(I)–NHC complexes were obtained as white solids.

2.4.1 Chloro[3-(2-(3,5-dimethyl-1*H*-pyrazol-1-yl)ethyl)-1-methyl-1*H*-imidazole-2-ylidene]silver(I) [$C_{11}H_{16}AgClN_4$], (2a). Yield 0.258 g, 94%, mp 213–215 °C. FT-IR: ν_{max}/cm^{-1} 1232 (CN). ^{1}H-NMR (600 MHz, $CDCl_3$) δ: 6.85 (d, J = 1.8 Hz, 1H), 6.41 (d, J = 1.8 Hz, 1H), 5.73 (s, 1H), 4.53 (t, J = 5.6 Hz, 2H), 4.27 (t, J = 5.6 Hz, 2H), 3.81 (s, 3H), 1.88 (s, 3H), 1.69 (s, 3H). ^{13}C-NMR (151 MHz, $CDCl_3$) δ: 180.65, 148.67, 140.12, 122.02, 121.87, 105.33, 104.82, 49.18, 38.86, 13.51, 10.62. LRMS (ESI): m/z calcd for cationic fragment of $[M–AgCl]^+$: 205.1453; found: 205.1535. Anal. calcd for $C_{11}H_{16}AgClN_4$: C, 38.01; H, 4.64; N, 16.12, found: C, 37.89; H, 4.58; N, 16.07.

2.4.2 Chloro[3-(2-(3,5-dimethyl-1*H*-pyrazol-1-yl)ethyl)-1-ethyl-1*H*-imidazole-2-ylidene]silver(I) [$C_{12}H_{18}AgClN_4$], (2b). Yield 0.35 g, 91%, mp 183–185 °C. FT-IR: ν_{max}/cm^{-1} 1383 (CN). ^{1}H-NMR (600 MHz, $CDCl_3$) δ: 6.91 (d, J = 1.7 Hz, 1H), 6.50 (d, J = 1.7 Hz, 1H), 5.72 (s, 1H), 4.55 (t, J = 7.3 Hz, 2H), 4.30 (t, J = 7.3 Hz, 2H), 4.13 (q, J = 7.9 Hz, 2H), 2.20 (s, 3H), 1.85 (s, 3H), 1.43 (t, J = 7.3 Hz, 3H). ^{13}C-NMR (151 MHz, $CDCl_3$) δ 179.29, 148.77, 140.11, 121.94, 120.24, 105.38, 51.65, 49.22, 47.10, 17.07, 13.53, 10.54. LRMS (ESI): m/z calcd for cationic fragment of $[M–AgCl]^+$: calculated: 219.1610, found: 219.1755. Anal. calcd for $C_{12}H_{18}AgClN_4$ C, 39.86; H, 5.02; N, 15.49, found: C, 39.81; H, 4.90; N, 15.38.

2.4.3 Chloro[3-(2-(3,5-dimethyl-1*H*-pyrazol-1-yl)ethyl)-1-benzyl-1*H*-imidazole-2-ylidene]silver(I) [$C_{17}H_{20}AgClN_4$], (2c). Yield 0.27 g, 88%, mp 201–203 °C. FT-IR: ν_{max}/cm^{-1} 1381 (CN). ^{1}H-NMR (600 MHz, $CDCl_3$) δ: 7.51–7.27 (m, 5H)), 6.85 (d, J = 7.4 Hz, 1H), 6.53 (d, J = 7.4 Hz, 1H), 5.69 (s, 1H), 5.25 (s, 2H), 4.59 (t, J = 5.4 Hz, 2H), 4.31 (t, J = 5.5 Hz, 2H), 2.19 (s, 3H), 1.78 (s, 3H). ^{13}C-NMR (151 MHz, $CDCl_3$) δ 180.59, 162.57, 148.77, 140.16, 135.51, 129.09, 128.67, 127.71, 122.28, 121.01, 105.32, 55.74, 51.67, 49.16, 13.55, 10.57. LRMS (ESI): m/z calcd for cationic fragment of $[M–AgCl]^+$: 281.1766, found: 281.1888. Anal. calcd for $C_{17}H_{20}AgClN_4$ C, 48.19; H, 4.76; N, 13.22, found: C, 48.10; H, 4.68; N, 13.13.

2.4.4 Chloro[3-(2-(3,5-dimethyl-1*H*-pyrazol-1-yl)ethyl)-1-methyl-1*H*-benzo[*d*]imidazole-2-ylidene]silver(I) [$C_{15}H_{18}AgClN_4$], (2d). Yield: 0.95 g, 92%, mp 225–228 °C. FT-IR: ν_{max}/

cm^{-1} 1388 (CN). ^{1}H-NMR (600 MHz, $CDCl_3$) δ: 7.4 (d, $J = 8.3$ Hz, 1H), 7.35 (d, $J = 8.3$ Hz, 1H), 7.28 (t, $J = 7.7$ Hz, 1H), 7.05 (t, $J = 7.7$ Hz, 1H)., 5.65 (s, 1H), 4.82 (t, $J = 5.7$ Hz, 2H), 4.46 (t, $J = 5.8$ Hz, 2H), 4.09 (s, 3H), 1.20 (s, 3H), 0.84 (s, 3H). ^{13}C-NMR (151 MHz, $CDCl_3$) δ: 188.35, 147.45, 139.74, 133.51, 133.17, 124.54, 124.50, 112.44, 112.32, 105.36, 49.38, 47.57, 44.17, 16.50, 13.87, 10.13. LRMS (ESI): m/z calcd for cationic fragment of $[M–AgCl]^+$: 255.1610, found: 255.1730. Anal. calcd for $C_{15}H_{18}AgClN_4$ C, 45.31; H, 4.56; N, 14.09, found: C, 45.23; H, 4.47; N,13.89.

2.4.5 Chloro[3-(2-(3,5-dimethyl-1*H*-pyrazol-1-yl)ethyl)-1-ethyl-1*H*-benzo[*d*]imidazole-2-ylidene]silver(I) [$C_{16}H_{20}AgClN_4$], (2e). Yield: 0.34 g, 89%, mp = 199–201 °C. FT-IR: ν_{max}/cm^{-1} 1398 (CN). ^{1}H-NMR (600 MHz, $CDCl_3$) δ: ^{1}H NMR (600 MHz, chloroform-*d*) δ 7.46 (d, $J = 8.2$ Hz, 1H), 7.43 (t, $J = 8.3$ Hz, 1H), 7.32 (t, $J = 8.3$, Hz, 1H), 7.20 (d, $J = 8.2$ Hz, 1H), 5.60 (s, 1H), 4.90 (t, $J = 7.2$ Hz, 2H), 4.44 (dt, $J = 23.5$, 6.2 Hz, 4H), 2.02 (s, 3H), 1.54 (s, 3H), 1.40 (t, $J = 7.2$ Hz, 3H). ^{13}C NMR (151 MHz, $CDCl_3$) δ 188.35, 147.45, 139.74, 133.51, 133.17, 124.54, 124.50, 112.44, 112.32, 105.36, 49.38, 47.57, 44.17, 16.50, 13.87, 10.13. LRMS (ESI): m/z calcd for cationic fragment of $[M–AgCl]^+$: 269.1766, found: 269.1878. Anal. calcd for $C_{16}H_{20}AgClN_4$ C, 46.68; H, 4.90; N, 13.61, found: C, 46.79; H, 5.03; N, 13.51.

2.5 *In vitro* antibacterial study of the compounds

Ten compounds (five salts and their Ag(I)–NHC complexes) were tested for antibacterial activity against four bacterial strains, two Gram-positive (*Staphylococcus aureus* and *Enterococcus faecalis*) and two Gram-negative (*Klebsiella pneumoniae* and *Pseudomonas aeruginosa*). The broth microdilution method, as described by Moodley *et al.* (2018), was employed to determine the percentage inhibition and IC_{50} values.[38] Briefly, the samples were serially diluted to obtain a concentration range of 6.25 to 200 μg mL^{-1}. Compounds **1a–e**, **2c**, and **2d** were diluted in 5% DMSO. **2a**, **2b**, and **2e** were diluted in 10% DMSO. All bacterial strains were grown in Mueller-Hinton Broth at pH 7.4 in a 30 °C incubator for 24 hours and adjusted to an OD equivalent to 0.5 McFarland's standard before aliquots of bacterial culture were added to the test samples. Samples with bacterial culture were incubated for 20 hours at 30 °C, followed by the addition of freshly prepared iodonitrotetratzolium chloride (2-(4-iodophenyl)-3-(4-nitrophenyl)-5-phenyl-2*H*-tetrazolium chloride). This was followed by an additional 4 hours of incubation at 30 °C and absorbance reading at 490 nm using a multimodal plate reader (Biotek Synergy HT, USA) with Gen 5 software (Biotek Synergy HT, USA Ver 2.01.14). All compounds were tested in triplicate on two separate occasions. The negative control was treated as per above, but contained bacterial cells exposed to 5% or 10% DMSO only, and this was used to represent 100% of live, metabolically active microbes. Statistical analysis was conducted using One-way ANOVA and the Tukey–Kramer post-test on GraphPad InStat software version 3.10 for Windows (GraphPad Software, San Diego, California, USA). Differences were considered significant when $p < 0.05$.

2.6 Computational studies

Geometry optimisation of the imidazolium salts was done using the Gaussian16 program.[39] Gauss View version 5 by Semichem, Inc.[40] was used to generate the input files and visualise the output. Density functional theory (DFT) calculations were performed using the B3LYP functional and the 6-31+G(d,p) basis set.[41] The LanL2DZ basis set was used for the Ag atom in the Ag(I)–NHC complexes.[42] A frequency calculation yielded the IR spectra and confirmed the structures were minima with no imaginary frequencies. The UV-visible spectra were obtained using the TDDFT keyword.[43] The TDDFT calculation also gave the frontier molecular orbital (FMO) energies, that is, the highest occupied molecular orbital (E_{HOMO}) and lowest unoccupied molecular orbital (E_{LUMO}).[44] These energies were used to determine the emission properties of the salts and the complexes and to estimate the quantum chemical descriptors. The descriptors included bandgap energy (ΔE) (eqn (1)), ionisation potential (IP) (eqn (2)),[45] global softness (S) (eqn (3)), chemical hardness (η) (eqn (4)),[45] electrochemical potential (μ) (eqn (5)),[45] electronegativity (χ) (eqn (6)),[45] and electrophilicity index (eqn (7)).[45] The *XYZ* coordinates of the optimised structures, including the simulated IR and UV-visible spectra, are available in the (SI) file.

$$\Delta E = E_{HOMO} - E_{LUMO} \quad (1)$$

$$IP = -E_{HOMO} \quad (2)$$

$$S = \frac{1}{\eta} \quad (3)$$

$$\eta = \frac{E_{LUMO} - E_{HOMO}}{2} \quad (4)$$

$$\mu = -\frac{IP + EA}{2} \quad (5)$$

$$\chi = -\mu \quad (6)$$

$$\omega = \frac{\mu^2}{2\eta} \quad (7)$$

Drug-likeness scores and bioactivity prediction were carried out using the online SwissDrugDesign program. SWISSADME predicted the following parameters: lipophilicity, water solubility, pharmacokinetics, and drug-likeness of the azolium salts that were used as ligand precursors for the synthesis of Ag(I)–NHC complexes.[46–48]

3. Results and discussion

3.1 Synthesis and characterisation of the azolium salts and Ag(I)–NHC complexes

The first reaction involved the formation of 3,5-dimethyl-1*H*-pyrazole from 2,4-pentanedione and hydrazine hydrate. The reaction proceeded through the nucleophilic attack of hydrazine on the two carbonyl groups of 2,4-pentanedione. The intermediate is a hydrazone, which undergoes ring closure to form a pyrazole ring.[49] *N*-Alkylation that involved the deprotonation of 3,5-dimethyl-1*H*-pyrazole, with the pyrazole nitrogen acting as a nucleophile, that attacked one of the carbon atoms

of 1,2-dichloroethane, produced 1-(2-chloroethyl)-3,5-dimethyl-1*H*-pyrazole. In the reaction, tetrabutylammonium chloride was the phase transfer catalyst. The nitrogen displaced the chlorine atom, forming the product 1-(2-chloroethyl)-3,5-dimethyl-1*H*-pyrazole. All the azolium salts were synthesised by the solvent-free method of reacting 1-(2-chloroethyl)-3,5-dimethyl-1*H*-pyrazole and the desired imidazole source under mild temperatures. The reaction proceeded *via* the S_N2 reaction route, where the halide on the 1-(2-chloroethyl)-3,5-dimethyl-1*H*-pyrazole was displaced by the lone pair of electrons on the sp^2 nitrogen in the substituted imidazole.[49] The wingtips N-substituents (R group, Scheme 1) were chosen as methyl, ethyl and benzyl.

The pyrazolyl functionalised imidazolium and benzimidazolium salts (**1a–e**) (Scheme 1) were obtained in high yields. Preliminary evidence for the successful synthesis of the azolium salts was seen as the appearance of an acidic imidazolium proton between 9 and 10 ppm in their ^{1}H-NMR spectra. The other two protons on the imidazolium moieties appeared as two doublets of one proton, each between 7 and 8 ppm for compounds **1a–c**. The presence of a substituted phenyl ring for compounds **1d** and **1e** gave rise to two doublets and two triplets for the four phenyl protons of the benzimidazolium salts.[32] The key characteristic signals on the ^{13}C-NMR were due to the imidazolium carbon atoms observed between 137 and 139 ppm (see SI Fig. S2–S11).

The Ag(I)–NHC complexes were obtained by reacting the imidazolium and benzimidazolium salts with Ag_2O in dichloromethane in the dark at room temperature (Scheme 1). Ag_2O is a weak (metal oxide) base often used as a Lewis acid to donate empty orbitals to electron-rich species.[50] The basic nature allows it to deprotonate the imidazolium salt for *in situ* carbene formation, where the silver(I) ion subsequently donates an empty orbital to the electron-rich carbene.[51] The complexes of the simple imidazolylidene ligands (**2a–c**) are unstable in air and moisture as they turn from white to brown hygroscopic solids. In contrast, the benzimidazolylidene-based **2d** and **2e** are stable in air and moisture due to the added stabilisation of the delocalised electrons of the fused phenyl ring.

Successful formation of the Ag(I)–NHC complexes was characterised by the loss of the acidic proton on the salt and the formation of the Ag–carbene bond, which is observed as a generally weak signal around 180 ppm for complexes **2a–c** and around 190 ppm in the ^{13}C NMR spectra of complexes **2d–e**.[52] The downfield shift of the imidazolium C2-carbon signals from 137–139 ppm to 180 and further down to 190 ppm also indicated the successful formation of the Ag(I)–C bond. However, in most cases, the Ag(I)–C signal appears weak in the ^{13}C NMR spectrum, and in some reported instances, it was not observable due to its lability.[26,53,54]

The experimental FT-IR spectra show the $\nu_{(CN)}$ bands for azolium salts **1a–e** at 1555, 1558, 1457, 1562 and 1563 cm^{-1}, respectively (see SI, Fig. S32–S41). All the salts are highly hygroscopic and imbibed varying quantities of water, as indicated by the broad peaks at around 3300 cm^{-1}, a commonly reported observation for the handling and storage of such salts.[55] The hygroscopic nature of the azolium salts also affected

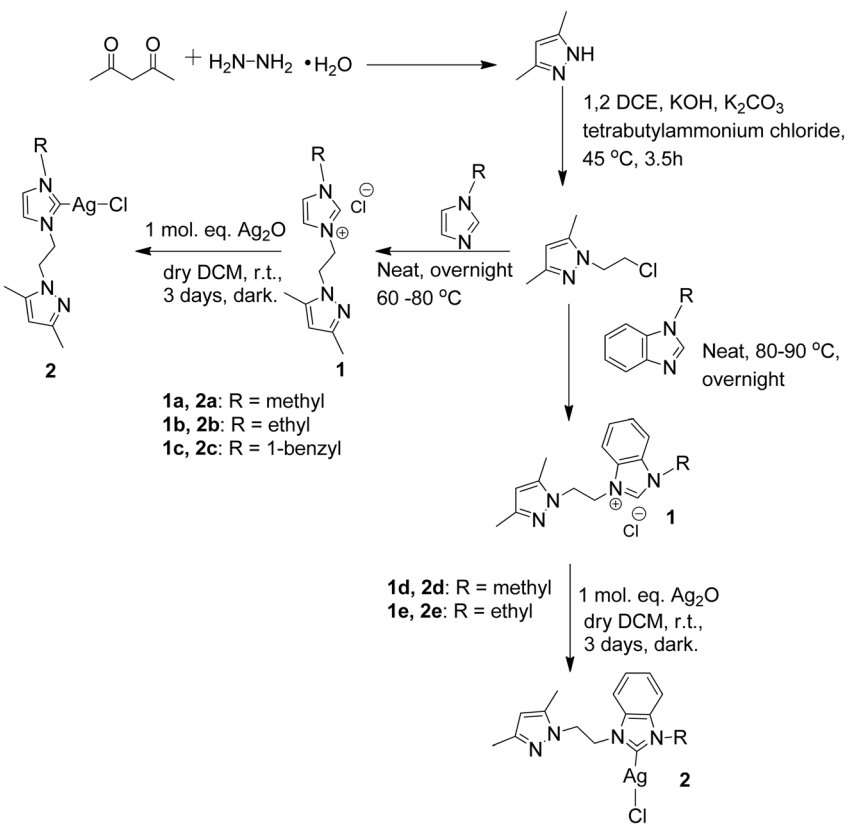

Scheme 1 Synthesis route for the azolium salts (**1a–e**) and the Ag(I)–NHC complexes (**2a–e**).

their elemental analysis data, which showed variable numbers of water molecules.[56] After complexion, the CN vibrations of the Ag(I)–NHC complexes, **2a–e**, shifted to lower energy regions, such as 1232, 1383, 1381, 1388 and 1398 cm^{-1}, respectively, due to the presence of the electropositive Ag(I) centre, which draws the electron density towards itself.[32] The simulated IR spectra of the azolium salts and their Ag(I)–NHC complexes showed bands in similar regions comparable to those of the experimental spectra (see SI, Fig. S32–S41). The simulated UV-vis spectra (see SI, Fig. S42–S51) show the absorption bands in the same regions (200–350 nm) as reported in the literature.[57] Elemental analysis showed that the synthesised Ag(I) complexes were coordinated to only one NHC ligand through the carbene (C2) carbon.

The calculated mass-to-charge ratios of the azolium salts gave comparable values to the experimental, indicating the successful synthesis of the proposed structures and the purity of the compounds. The most intense fragments belonged to the molecular ion peaks, representing the molecular weight of the cationic fragments of the salts. The mass spectrometry results of the complexes showed that the Ag(I) complexes were ionised on the Ag(I)–carbene bond, forming the positive ion (which is the imidazolium salt) and the negative counterion comprising the silver and chloride ions (–Ag–Cl).[54] Thus, the spectroscopic and analytical data confirm the successful synthesis and isolation of the proposed compounds in high bulk purity.

3.2 *In vitro* antibacterial studies of the compounds 1a–e and complexes 2a–e

The antibacterial efficacy of the synthesised salts (**1a–e**) and their corresponding Ag(I)–NHC complexes (**2a–e**) was tested by studying their inhibition of two Gram-negative (*K. pneumoniae* and *P. aeruginosa)* and two Gram-positive bacterial strains (*S. aureus* and *E. faecalis*) at concentrations of 200, 100, 50, 25 and 12.5 μg mL^{-1}. Statistical analysis was carried out, and it was concluded that almost all the compounds had a significant inhibition at the highest concentration of 200 μg mL^{-1}. Neomycin, an antibacterial drug used as the standard, belongs to a class of antibiotics known as aminoglycosides, which inhibit bacterial protein synthesis, resulting in cell death. The antibiotic is most effective at inhibiting Gram-negative bacteria (*K. pneumoniae* and *P. aeruginosa*) due to its ability to penetrate their thinner outer membrane compared to the thicker one of Gram-positive strains.[58] Neomycin also exhibits notable activity against the Gram-positive bacterial strains (*S. aureus* and *E. faecalis*), but its clinical utility is limited by resistance mechanisms.[59]

A comparative evaluation of the antibacterial activity of the imidazolium salts (**1a–e**) and the corresponding Ag(I)–NHC complexes (**2a–e**) (Table 1) revealed that the complexes consistently exhibited superior bacterial inhibition. Enhancement of activity upon complexation is similar to previous studies, which have reported that Ag(I)–NHC complexes demonstrated significantly greater antibacterial efficacy than their precursor salts.[60–62] This is supported by the well-established antibacterial activity of silver, which is known to be a good agent for disrupting the bacterial cell wall and inhibiting DNA replication, resulting in reduced enzymatic activity and cell death.[63–65] It is noteworthy that all the Ag(I) compounds showed significantly better or comparable antimicrobial activity than neomycin against all the tested bacteria strains. Also, all the compounds statistically exhibited comparable activities showing that the presence of a benzimidazolium moiety in **2d** and **2e** did not increase antibacterial activity.

Compound **2b** is especially worth mentioning, because it showed a significantly high percentage inhibition of 59% at a lower concentration of 50 μg mL^{-1} compared to neomycin with 44% at 200 μg mL^{-1} against *S. aureus*.[66] It also did better against *E. faecalis*, a common cause of hospital-acquired infections, accounting for 60% of reported cases.[67] Neomycin showed 63% inhibition, lower than the least active complex, **2d** (74%), against the deadly microbe. The better activity of the complexes than neomycin, a broad-spectrum standard antibiotic,[68] against both Gram-positive strains showed the potential efficacy of these Ag(I)–NHC as antibacterial agents.

The good activity of the complexes against *K. pneumoniae* was indicated by the fact that all had inhibitions ranging between 84–93%, comparable to the 89% of neomycin. When tested against *P. aeruginosa*, the complexes showed better bacterial

Table 1 Highest percentage inhibition of the azolium salts (**1a–e**) and their Ag(I)–NHC complexes (**2a–e**)[a]

	Gram-positive		Gram-negative	
Compound	*S. aureus*	*E. faecalis*	*K. pneumoniae*	*P. aeruginosa*
1a	15.11 (±7.55)	19.55 (±7.14)	13.56 (±4.07)	2.52 (±2.18)
1b	17.90 (±12.81)	0.50 (±6.27)	3.70 (±6.80)	4.50 (±1.36)
1c	10.67 (±3.92)	3.06 (±8.54)	28.56 (±3.67)	4.46 (±8.68)
1d	24.29 (±9.03)	1.67 (±1.87)	23.26 (±4.55)	3.38 (±3.63)
1e	18.06 (±5.54)	29.88 (±5.85)	5.70 (±2.68)	7.04 (±3.67)
2a	61.04 (±5.46)	81.32 (±8.55)	84.67 (±8.67)	85.46 (±5.49)
2b	59.01 (50) (±2.23)	91.02 (50) (±0.57)	85.60 (±3.61)	81.34 (±5.37)
2c	60.77 (±4.85)	86.71 (±2.12)	93.02 (±1.08)	83.97 (±5.49)
2d	59.53 (±3.87)	73.69 (±3.92)	90.00 (±1.87)	80.16 (±6.57)
2e	51.61 (±5.56)	90.72 (±0.97)	88.79 (±1.48)	96.53 (±7.51)
Neomycin	44.19 (±3.84)	63.07 (±7.32)	89.02 (±1.79)	44.41 (±9.37)

[a] All data reported at 200 μg mL^{-1} concentration (unless noted otherwise).

inhibition (80–87%) than the 44% for the control drug, neomycin. Cumulatively, these results show the promising antibacterial efficacy of the five Ag(I)–NHC complexes presented in this report. In context, the antibacterial activity of the five Ag(I)–NHC complexes was comparable to that reported by Atli and Aksu Their Ag(I)–NHC complexes with MIC values against *P. aeruginosa* in the range 0.61–1.25 mg mL^{-1}, but were more sensitive against *S. aureus* with an MIC of 0.61 μg mL^{-1}.[69] Mnasri *et al.* reported complexes with better activity than ours, and had MIC values between 0.24 and 125 μg mL^{-1} against *S. aureus*.[26] One of the best reported Ag(I)–NHC complexes by Tutar and Celik is based on benzimidazole with an MIC of 15.6 μg mL^{-1} against *S. aureus* and *E. faecalis*.[70]

Furthermore, the antibacterial activity of the Ag(I)–NHC complexes was evaluated using the half-maximal inhibitory concentration (IC_{50}) method based on the molar concentrations of the compounds (Table 2) to study some potential structure–activity relationships. Overall, the complexes exhibited greater efficacy against the Gram-negative strains than the Gram-positive strains, due to the thinner peptidoglycan layer in the Gram-negative cell wall, allowing easy penetration by antibacterial agents.[71] The activity of complexes **2a–e** shows a distinct structure–activity relationship (SAR) influenced by either the nature of the N-substituent (R group) or the backbone of the azolium moiety. The increase in activity is based on changes in steric bulk and lipophilicity of the complexes due to the alkyl N-substituents. This is exhibited by **2c**, which is the most potent with low IC_{50} values against both Gram-positive (*S. aureus* = 197 μM; *E. faecalis* = 20 μM) and Gram-negative strains (*K. pneumoniae* = 26 μM; *P. aeruginosa* = 62 μM). The enhanced activity of **2c** can be attributed to increased lipophilicity facilitated by the aromatic substituent. Increasing the chain of the alkyl group from methyl (**2a**) to ethyl (**2b**) decreased the activity of the complex against the Gram-positive strains; however, it did improve the potency of the benzimidazolium-based counterpart (**2e** *vs.* **2d**). The two complexes with an ethyl N-substituent group (**2b** and **2e**) showed better activity against the Gram-negative strains than related ones (**2a** and **2d)** bearing the smaller methyl group.

Thus, it can be suggested that the longer carbon chain enhanced lipophilicity, and reports have shown that complexes with long alkyl chain N-substituents have a slower release rate of metal ions than those with shorter carbon chains, which enhanced the antibacterial activity of complexes **2b** and **2e** against the Gram-negative strains.[72] These results are consistent with reports showing that antibacterial activity depends on a combination of factors and is generally strain dependent, and different bacteria respond differently to the same antibacterial agents.[73] Thus, the activity of the compounds should be analysed separately against each strain. However, fine-tuning the NHC ligand structure can lead to enhanced antimicrobial properties for Ag(I)–NHC complexes, particularly against resistant Gram-negative strains.

Table 2 IC_{50} (μM) of the Ag(I)–NHC complexes against the tested bacterial strains

	Gram-positive		Gram-negative	
Compound	*S. aureus*	*E. faecalis*	*K. pneumoniae*	*P. aeruginosa*
2a	296	103	161	136
2b	323	133	88	107
2c	197	20	26	62
2d	443	272	125	155
2e	419	108	60	98
Neomycin	21	8	276	77

3.3 Computational study

3.3.1 Chemical reactivity descriptors. In this study, DFT calculations were carried out to get insight into the reported compounds' structure-chemical reactivity properties (Table 3). The energy difference between the lowest unoccupied molecular orbital (LUMO) and the highest occupied molecular orbital (HOMO), ΔE ($E_{LUMO} - E_{HOMO}$), was calculated according to eqn (1). The HOMO and LUMO levels are critical for electron mobility, which is related to the compound's biological activity.[74] The HOMO is the preferred location for oxidation, whereas the LUMO is where the molecule is most likely to be reduced; hence, the compound has superior biological activity when the HOMO is located primarily on the donor atoms, and the LUMO is located on the acceptor atoms.[75] The smaller the HOMO–LUMO energy gap, the greater the compound's

Table 3 Chemical reactivity descriptors for the reported compounds[a]

	HOMO	LUMO	ΔE	IP	S	η	μ	χ	ω
1a	−9.130	−5.093	4.037	9.130	0.495	2.022	−7.112	7.112	12.529
1b	−9.097	−4.991	4.105	9.097	0.487	2.053	−7.044	7.044	12.087
1c	−9.032	−4.850	4.182	9.032	0.478	2.091	−6.941	6.941	11.523
1d	−9.129	−5.293	3.836	9.129	0.521	1.918	−7.211	7.211	13.555
1e	−9.099	−5.224	3.875	9.098	0.516	1.938	−7.161	7.161	13.233
2a	−6.050	−0.993	5.057	6.050	0.396	2.528	−3.521	3.521	2.452
2b	−6.034	−0.972	5.062	6.034	0.395	2.531	−3.502	3.502	2.424
2c	−6.052	−1.225	4.827	6.052	0.414	2.414	−3.638	3.638	2.742
2d	−6.347	−1.880	4.467	6.347	0.448	2.234	−4.113	4.113	3.787
2e	−6.093	−1.875	4.218	6.093	0.474	2.109	−3.984	3.984	3.763

[a] ΔE is the HOMO–LUMO energy gap, S is global softness, I is ionisation potential, η is global hardness, μ is chemical potential, χ is electronegativity, and ω is electrophilicity index.

potential for biological activity, as it allows for better electron mobility.[76] In contrast, a larger ΔE value indicates high stability and low chemical reactivity.[77]

The HUMO–LUMO analysis shows that the benzimidazolium salts have a smaller energy gap and should have better activity than the imidazolium salts. The antibacterial activity of **2d** and **2e** (Tables 1 and 2) can be ascribed to the presence of the benzene ring, which stabilises the entire benzimidazolium moiety and controls the steady release of the Ag(I) ions.[21] Based on the HOMO–LUMO energy gap, the order of activity is **1d** > **1e** > **1b** > **1a** > **1c**. From Table 3, the imidazolium and benzimidazolium salts have smaller HOMO–LUMO energy gaps than the corresponding Ag(I) complexes. Thus, the order of activity for the complexes based on the HOMO–LUMO energy gap is **2e** > **2d** > **2c** > **2a** > **2b**.

The order of activity against the different strains based on their IC_{50} values for *S. aureus* is **2c** > **2b** > **2a** > **2e** > **2d**; for *E. faecalis* is **2c** > **2a** > **2e** > **2b** > **2d**; for *K. pneumoniae* is **2c** > **2e** > **2b** > **2d** > **2a** and for *P. aeruginosa* is **2c** > **2b** > **2e** > **2a** > **2d**. Complexes **2d** and **2e** have the smallest HOMO–LUMO energy gap, indicating that the benzimidazole is more favourable than the simple imidazole. With the exception of **2c**, the benzimidazolium-based complexes were generally more active than the imidazolium-based ones, confirming the HOMO–LUMO prediction that **2d** and **2e** have smaller energy gaps than **2a** and **2b**. This is despite the fact that the *in vitro* antibacterial activity is strain-sensitive. Serdaroğlu and coworkers also reported that their NHC precursor had a smaller HOMO–LUMO energy gap (4.3522 eV) than its Ag(I)–NHC complex (5.1704 eV). However, the Ag(I)–NHC complex exhibited better antibacterial activity than the salt.[37]

Global softness, hardness, and ΔE can be used to predict compound stability. A big energy gap and high global hardness value indicate a more stable compound with reduced biological activity.[78] Global hardness is defined as the resistance to charge transfer, while global softness demonstrates the compound's susceptibility to charge transfer. The order of stability of the five salts is **1c** > **1b** > **1a** > **1d** > **1e**, while the order for the Ag(I) complexes is **2b** > **2a** > **2c** > **2d** > **2e**. Based on the global hardness values for the complexes, the most active complex is **2e**, followed by **2d**, with **2b** and **2a** being the least active, while compound **2c** lies in between. However, the IC_{50} values showed compound **2c** as the most active against all the bacterial strains.

Since the activity of the complexes is strain-sensitive, it is not easy to link the DFT predictions to the *in vitro* evaluations, and numerous investigations have examined frontier molecular orbital maps to ascertain the possible reactivity of molecules.[79] None of the salts exhibited *in vitro* antibacterial activity similar to that of the Ag(I)–NHC complexes (**2a–e**), despite the salts' global softness being on par with, and occasionally even better

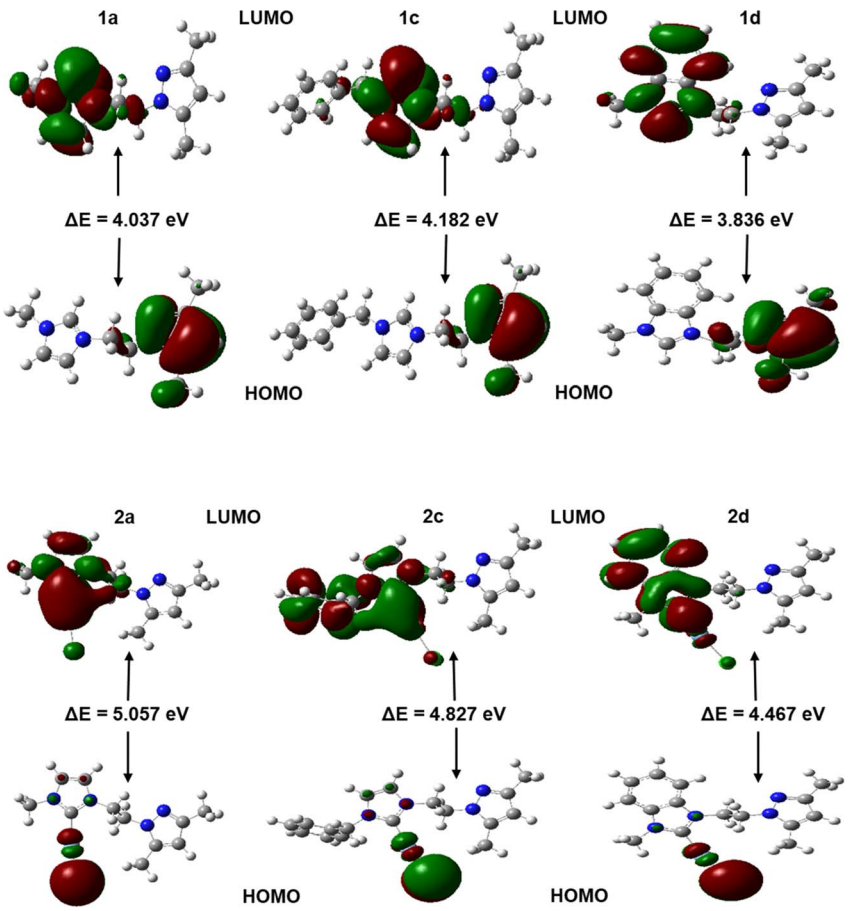

Fig. 1 FMOs of selected salts (**1a**, **1c** and **1d**) and their Ag(I)–NHC complexes (**2a**, **2c** and **2d**).

than, that of the complexes. This implies that although DFT is a useful tool for predicting a compound's reactivity, experimental results must always be utilised to confirm the predictions.[80]

The lower ionisation energies and electronegativity values for the Ag(I)–NHC complexes compared to the salts indicate that less energy is required to remove electrons, implying improved electron-donating ability and activity.[81] The electrophilicity

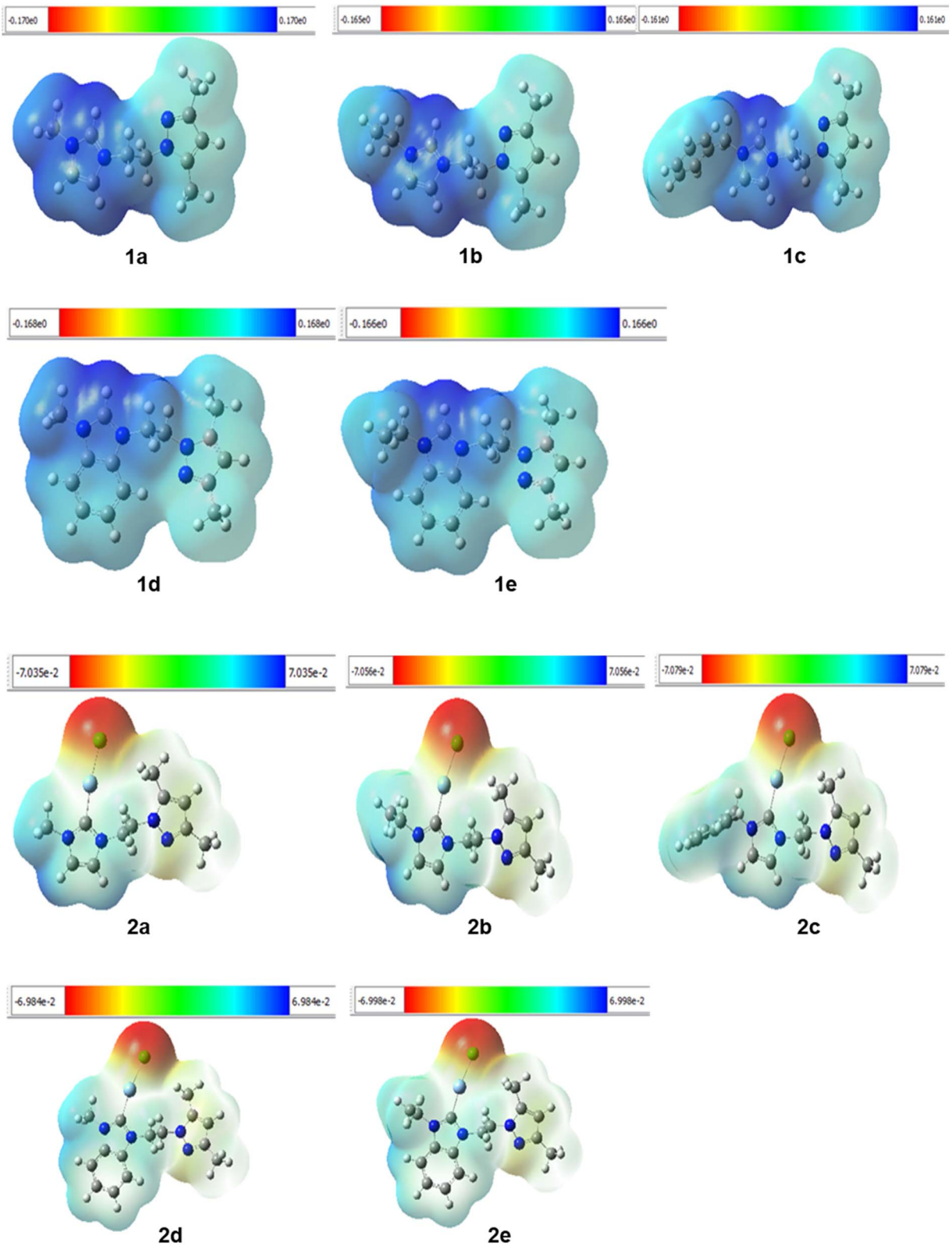

Fig. 2 MEP surfaces of compounds 1a–e and 2a–e.

Table 4 Computational SWISS ADME prediction of compounds[a] 2a–e

Compound	Consensus log $P_{o/w}$	Water solubility (mg mL^{-1})	P-gp substrate	Lipinski
2a	0.83	0.179	No	Yes, 0 violations
2b	1.11	0.108	No	Yes, 0 violations
2c	1.96	0.0084	Yes	Yes, 0 violations
2d	1.90	0.0087	Yes	Yes, 0 violations
2e	2.17	0.0053	Yes	Yes, 0 violations

[a] Log *P*: lipophilicity. Water solubility was calculated using the ESOL method a quantitative structure–property relationship (QSPR)-based model.

index measures the ability of a compound to accept electrons. The higher the electrophilicity index, the greater the electron acceptance. Thus, compounds **1a–e** are better electron acceptors, while **2a–e** are good electron donors. It may be concluded that while compounds **2a–e** have larger energy gaps than **1a–e**, their softness and ability to readily donate electrons give the Ag(I)–NHC complexes superior *in vitro* antibacterial activity over the azolium salts.[82]

The FMO analysis of the salts showed that the LUMO orbitals are situated on the imidazolium moiety, while the HOMO orbitals are on the pyrazole moiety (Fig. 1). Thus, the imidazolium moiety acts as the electron acceptor, while the pyrazole donates the electrons.[75] For the Ag(I)–NHC complexes, the LUMO is primarily on the imidazolium moiety and slightly on the silver and chlorine atoms, while the HOMOs are on the silver and chlorine atoms. Thus, in the Ag(I)–NHC complexes, the chlorine and silver atoms can both donate and accept electrons. The high HOMO and LUMO energies of the Ag(I)–NHC complexes compared to their respective salts showed that the metal complexes are better electron donors and thus have better *in vitro* activity than the salts.[81]

3.3.2 Molecular electrostatic potential analysis. The 3-D molecular electrostatic potential (MEP) maps are useful for locating the sites where nucleophilic and electrophilic attacks may occur. Electronegative groups usually have negative potentials due to their ability to attract bonding electrons.[83,84] The positive potential in blue is the region where electrophilic attacks occur. The red region designates a negative potential and area for nucleophilic attack.[85] In Fig. 2, compounds **1a–e** are more electrophilic as denoted by the blue regions that lie over the imidazolium moieties. The LUMO (Fig. 1) on the imidazolium moieties of compounds **1a–e** further supports this, demonstrating that these areas are electron acceptors.[86] MEP surfaces for the Ag(I)–NHC complexes indicated a negative potential centred on the chlorine atom, the most electronegative in the compounds. Thus, the MEP analysis is consistent with the FMO study, which revealed that the HOMO of the complexes is exclusively located on the silver and chlorine atoms. The slight prevalence of a positive potential in compounds **2a–e** indicates that they are more vulnerable to a nucleophilic rather than an electrophilic attack.[87]

3.3.3 SWISSADME prediction. SwissDrugDesign was used to estimate the ligand precursors' lipophilicity, water solubility, pharmacokinetics, and drug-likeness. Log $P_{o/w}$ is a measure of a compound's lipophilicity, or how easily it dissolves in a fatty environment like a cell membrane. According to Lipinski's rule of five, a drug-like molecule should have a log *P* value smaller than five in order to ensure adequate aqueous solubility and absorption.[46] It has been demonstrated that a compound's antibacterial activity varies with the length of its carbon chain, with longer chains showing greater activity than shorter ones. This happens because the longer carbon chains increase the compound's lipophilicity, which makes it easier to cross the bacterial cell membrane.[68,88]

Among the investigated log $P_{o/w}$ values (Table 4) of the complexes, the best lipophilicity was for **2e**, which consists of an ethyl substituent on the benzimidazolium moiety. The good lipophilicity of compound **2c** can be linked to its good antibacterial activity, which is exhibited by the best IC_{50} values across all the tested strains. Complex **2e** had the second-best IC_{50} values against *E. faecalis*, *K. pneumoniae*, and *P. aeruginosa* (Table 2), thus also showing the role played by its good lipophilicity.

When compounds **2a** and **2d** are compared to compounds **2b** against **2e**, it is clear that the benzimidazolium moiety increased the compounds' lipophilicity. The log $P_{o/w}$ value of **2c** indicated that the benzyl moiety is more lipophilic than methyl and ethyl groups. Compounds **2c–e** were identified as potential P-gp substrates that use the P-glycoprotein transporter to cross the cell membrane.[89] As a result, due to their high lipophilicity, these compounds can easily permeate the bacterial cell membrane.

4. Conclusion

In this work, imidazolium and benzimidazolium-based salts and their Ag(I)–NHC complexes were synthesised, and their *in vitro* antibacterial and computational studies were conducted. The Ag(I)–NHC complexes showed better antibacterial activity than their respective salts and the control drug, neomycin. The antibacterial studies showed that the percentage inhibition of the compounds depended, to a large extent, on the concentration of the compound. DFT predicted the benzimidazolium-based Ag(I)–NHC complexes to be better than the imidazolium-based ones. The Ag(I)–NHC complexes were predicted to be better electron donors than their respective salts due to the presence of the silver and chlorine atoms. However, the IC_{50} results showed that the imidazolium-based Ag(I)–NHC complex with a benzyl N-substituent exhibited the best activity, and this was supported by the SWISSADME prediction, which

showed the ligand precursor of the same complex to have good lipophilicity. The results showed that the benzimidazolium moiety and a longer carbon chain increased antibacterial activity. Fine-tuning the NHC ligand structure can enhance the antimicrobial properties of Ag(I)–NHC complexes, particularly against strains that have developed resistance to currently available drugs. Thus, future considerations should prioritise altering the chain length of the carbon N-substituent of especially benzimidazolium-based Ag(I) complexes.

Conflicts of interest

There are no conflicts of interest to declare.

Abbreviations

ADME	Absorption, distribution, metabolism and excretion
DFT	Density functional theory
DMSO	Dimethyl sulfoxide
FMO	Frontier molecular orbital
HOMO	Highest occupied molecular orbital
LUMO	Lowest unoccupied molecular orbital
IC_{50}	Half-maximal inhibitory concentration
MEP	Molecular electrostatic potential
MIC	Minimum inhibitory concentration
MRSA	Methicillin-resistant *Staphylococcus Aureus*
NHC	N-Heterocyclic Carbene
NMR	Nuclear magnetic resonance
SAR	Structure–activity relationship

Data availability

The data supporting this article have been included as part of the supplementary information (SI). Supplementary information: experimental and simulated spectra as well as the *XYZ* coordinates. See DOI: https://doi.org/10.1039/d5ra05570a.

Acknowledgements

The authors thank the National Research Foundation of South Africa and the University of KwaZulu-Natal for financial support. TS thanks the National Research Foundation of South Africa for a Competitive Programme for Rated Researchers grant [CPRR230527110705]. TS and NR acknowledge the Centre for High Performance Computing (CHPC), Cape Town, South Africa, for the computational resources.

References

1 A. B. G. Lansdown, Silver in Health Care: Antimicrobial Effects and Safety in Use, *Curr. Probl. Dermatol.*, 2006, **33**, 17–34, DOI: 10.1159/000093928.
2 S. H. Sumrra, W. Zafar, M. Imran and Z. H. Chohan, A Review on the Biomedical Efficacy of Transition Metal Triazole Compounds, *J. Coord. Chem.*, 2022, **75**(3–4), 293–334, DOI: 10.1080/00958972.2022.2059359.
3 M. Rendosova, R. Gyepes, I. C. Maruscakova, D. Mudronova, D. Sabolova, M. Kello, M. Vilkova, M. Almasi, V. Huntosova, O. Zemek and Z. Vargova, An: In Vitro Selective Inhibitory Effect of Silver(I) Aminoacidates against Bacteria and Intestinal Cell Lines and Elucidation of the Mechanism of Action by Means of DNA Binding Properties, DNA Cleavage and Cell Cycle Arrest, *Dalton Trans.*, 2021, **50**(3), 936–953, DOI: 10.1039/d0dt03332d.
4 F. M. Nareetsile, J. T. P. Matshwele and S. Odisitse, Metallo-Drugs as Promising Antibacterial Agents and Their Modes of Action, *J. Med. Chem. Sci.*, 2022, **5**, 1109–1131, DOI: 10.26655/JMCHEMSCI.2022.6.24.
5 H. D. Betts, C. Whitehead and H. H. Harris, Silver in Biology and Medicine: Opportunities for Metallomics Researchers, *Metallomics*, 2021, **13**(1), 1–12, DOI: 10.1093/mtomcs/mfaa001.
6 A. B. G. Lansdown, Silver in Health Care: Antimicrobial Effects and Safety in Use in Biofunctional Textiles and the Skin, *Curr. Probl. Dermatol.*, 2006, **33**, 17–34, DOI: 10.1159/000093928.
7 P. Cant, Silver (I) -N-Heterocyclic Carbene Complexes Challenge Cancer; Evaluation of Their Anticancer Properties and in Silico Studies, *Drug Dev. Res.*, 2021, 1–20, DOI: 10.1002/ddr.21822.
8 J. Gravel and A. R. Schmitzer, Imidazolium and Benzimidazolium-Containing Compounds: From Simple Toxic Salts to Highly Bioactive Drugs, *Org. Biomol. Chem.*, 2017, **15**(5), 1051–1071, DOI: 10.1039/C6OB02293F.
9 A. Frei, J. Zuegg, A. G. Elliott, M. Baker, S. Braese, C. Brown, F. Chen, G. C. Dowson, G. Dujardin, N. Jung, A. P. King, A. M. Mansour, M. Massi, J. Moat, H. A. Mohamed, A. K. Renfrew, P. J. Rutledge, P. J. Sadler, M. H. Todd, C. E. Willans, J. J. Wilson, M. A. Cooper and M. A. T. Blaskovich, Metal Complexes as a Promising Source for New Antibiotics, *Chem. Sci.*, 2020, **11**(10), 2627–2639, DOI: 10.1039/c9sc06460e.
10 A. Gautam, A. Gupta, P. Prasad and P. K. Sasmal, Development of Cyclometalated Iridium (III) Complexes of 2-Phenylbenzimidazole and Bipyridine Ligands for Selective Elimination of Gram-Positive Bacteria, *Chem.–Asian J.*, 2025, **20**(2), e202401060, DOI: 10.1002/asia.202401060.
11 H. Y. Huang, R. Y. Xue, S. X. Xiao, L. T. Huang, X. W. Liao, J. T. Wang, X. M. Duan, R. J. Yu and Y. S. Xiong, AIE-based ruthenium complexes as photosensitizers for specifically photo-inactivate gram-positive bacteria, *J. Inorg. Biochem.*, 2025, **262**, e112755, DOI: 10.1016/j.jinorgbio.2024.112755.
12 S. Kamat and M. Kumari, Emergence of Microbial Resistance against Nanoparticles: Mechanisms and Strategies, *Front. Microbiol.*, 2023, **14**, e1102615, DOI: 10.3389/fmicb.2023.1102615.
13 A. Kędziora, R. Wieczorek, M. Speruda, I. Matolínová, T. M. Goszczyński, I. Litwin, V. Matolín and G. Bugla-Płoskońska, Comparison of Antibacterial Mode of Action of Silver Ions and Silver Nanoformulations With Different Physico-Chemical Properties: Experimental and

Computational Studies, *Front. Microbiol.*, 2021, **12**, 1–12, DOI: 10.3389/fmicb.2021.659614.

14 A. Sanchez, C. J. Carrasco, F. Montilla, E. Alvarez, A. Galindo, M. Perez-Aranda, E. Pajuelo and A. Alcudia, Antimicrobial Properties of Amino-Acid-Derived N-Heterocyclic Carbene Silver Complexes, *Pharmaceutics*, 2022, **14**, e14040748, DOI: 10.3390/pharmaceutics14040748.

15 Q. L. Feng, J. Wu, G. Q. Chen, F. Z. Cui, T. N. Kim and J. O. Kim, A mechanistic study of the antibacterial effect of silver ions on *Escherichia coli* and *Staphylococcus aureus*, *J. Biomed. Mater. Res.*, 2000, **52**, 662–668, DOI: 10.1002/1097-4636(20001215)52:4<662::AID-JBM10>3.0.CO.

16 Y. Matsumura, K. Yoshikata, S. I. Kunisaki and T. Tsuchido, Mode of Bactericidal Action of Silver Zeolite and Its Comparison with That of Silver Nitrate, *Appl. Environ. Microbiol.*, 2003, **69**, 4278–4428, DOI: 10.1128/AEM.69.7.4278-4281.2003.

17 A. K. Mishra, V. Gautam, A. Gupta, R. Bansal, P. Bansal, S. Kumar and V. Gupta, Synthesis and antimicrobial activity of some newer benzimidazole derivatives – an overview, *J. Pharm. Res.*, 2010, **3**(2), 371–378.

18 O. Esarte, A. L. Cunningham, B. W. Davies and R. A. Jones, Antibacterial Thiamine Inspired Silver (I) and Gold (I) N-Heterocyclic Carbene Compounds, *Inorg. Chim. Acta*, 2021, **517**, e120152, DOI: 10.1016/j.ica.2020.120152.

19 R. A. Haque, M. A. Iqbal, S. Budagumpi, M. B. Khadeer Ahamed, A. M. S. Abdul Majid and N. Hasanudin, Binuclear Meta-Xylyl-Linked Ag(I)-N-Heterocyclic Carbene Complexes of N-Alkyl/Aryl-Alkyl-Substituted Bis-Benzimidazolium Salts: Synthesis, Crystal Structures and in Vitro Anticancer Studies, *Appl. Organomet. Chem.*, 2013, **27**(4), 214–223, DOI: 10.1002/aoc.2953.

20 M. O. Karataş, N. Özdemir, M. Sariman, S. Günal, E. Ulukaya and İ. Özdemir, Water-Soluble Silver(I) Complexes with N-Donor Benzimidazole Ligands Containing an Imidazolium Core: Stability and Preliminary Biological Studies, *Dalton Trans.*, 2021, **50**(33), 11596–11603, DOI: 10.1039/d1dt02008k.

21 S. Budagumpi, R. A. Haque, S. Endud, G. U. Rehman and A. W. Salman, Biologically Relevant Silver(I)-N-Heterocyclic Carbene Complexes: Synthesis, Structure, Intramolecular Interactions, and Applications, *Eur. J. Inorg. Chem.*, 2013, **25**, 4367–4388, DOI: 10.1002/ejic.20130048.

22 N. A. Johnson, M. R. Southerland and W. J. Youngs, Recent Developments in the Medicinal Applications of Silver-NHC Complexes and Imidazolium Salts, *Molecules*, 2017, **22**(8), 1–20, DOI: 10.3390/molecules22081263.

23 M. Kaloğlu, N. Kaloğlu, S. Günal and İ. Özdemir, Synthesis of N-Heterocyclic Carbene-Based Silver Complexes and Their Antimicrobial Properties against Bacteria and Fungi, *J. Coord. Chem.*, 2021, **74**(17–20), 3031–3047, DOI: 10.1080/00958972.2021.2014457.

24 D. Bensalah, N. Gurbuz, I. Ozdemir, R. Gatri, L. Mansour and N. Hamdi, Synthesis, Characterization, Antimicrobial Properties, and Antioxidant Activities of Silver-N-Heterocyclic Carbene Complexes, *Bioinorg. Chem. Appl.*, 2023, e3066299, DOI: 10.1155/2023/3066299.

25 A. Mnasri, A. Mejri, S. M. Hazmy, N. Hamdi and Y. Arfaoui, Silver–N-Heterocyclic Carbene Complexes- catalyzed Multicomponent Reactions Synthesis Spectroscopic Characterization, Density Functional Theory Calculations, and Antibacterial Study, *Arch. Pharm.*, 2021, e2100111, DOI: 10.1002/ardp.202100111.

26 M. Z. Ghdhayeb, K. J. Sabah, A. Washeel and M. Mohammed, New Ag (I) and Pd (II) Complexes Derived from Symmetrical and Asymmetrical NHC Precursors: Synthesis, Characterisation, Antibacterial Activity, and Theoretical Calculations, *J. Mol. Struct.*, 2021, **1245**, e131254, DOI: 10.1016/j.molstruc.2021.131254.

27 J. J. Liu, M. Y. Zhao, X. Zhang, X. Zhao and H. L. Zhu, Pyrazole derivatives as antitumor, anti-inflammatory and antibacterial agents, *Mini-Rev. Med. Chem.*, 2013, **13**, 1957–1966, DOI: 10.2174/13895757113139990078.

28 C. Pitchumani Violet Mary, R. Shankar and S. Vijayakumar, Theoretical Insights into the Metal Chelating and Antimicrobial Properties of the Chalcone Based Schiff Bases, *Mol. Simul.*, 2019, **45**(8), 636–645, DOI: 10.1080/08927022.2019.1573370.

29 J. C. Pessoa, M. F. A. Santos, I. Correia, D. Sanna, G. Sciortino and E. Garribba, Binding of Vanadium Ions and Complexes to Proteins and Enzymes in Aqueous Solution, *Coord. Chem. Rev.*, 2021, **449**, e214192, DOI: 10.1016/j.ccr.2021.214192.

30 G. L. Sasahara, F. S. Gouveia Júnior, R. de O. Rodrigues, D. S. Zampieri, S. G. da C. Fonseca, R. de C. R. Gonçalves, B. R. Athaydes, R. R. Kitagawa, F. A. Santos, E. H. S. Sousa, A. T. Nagao-Dias and L. G. de F. Lopes, Nitro-Imidazole-Based Ruthenium Complexes with Antioxidant and Anti-Inflammatory Activities, *J. Inorg. Biochem.*, 2020, **206**, e111048, DOI: 10.1016/j.jinorgbio.2020.111048.

31 M. Reddi, C. Rao and A. Murthy, Chemistry of Heterocycles. Part 9. Synthesis of Isoxazolylpyrazolones, *Chem. Informationsdienst*, 1986, **17**(11), 219–221.

32 H. M. Lee, P. L. Chiu, C. H. Hu, C. L. Lai and Y. C. Chou, Synthesis and structural characterisation of metal complexes based on pyrazole/imidazolium chlorides, *J. Org. Chem.*, 2005, **690**, 403–414, DOI: 10.1016/j.jorganchem.2004.09.053.

33 M. J. Saif and K. R. Flower, A general method for the preparation of N-heterocyclic carbene–silver(I) complexes in water, *Transition Met. Chem.*, 2013, **38**, 113–118, DOI: 10.1007/s11243-012-9667-3.

34 H. Ibrahim and M. D. Bala, Improved Methods for the Synthesis and Isolation of Imidazolium Based Ionic Salts, *Tetrahedron Lett.*, 2014, **55**(46), 6351–6353, DOI: 10.1016/j.tetlet.2014.09.116.

35 K. K. Bhasin, S. Pundir, S. Neogy, D. Mehta and S. K. Mehta, Synthesis, Characterisation and Structural Aspects of Some Symmetrical Organotellurium Halides Based on Bis(2-(3,5-Dimethyl-1H-Pyrazol-1-Yl)Ethyl)Telluride, *Phosphorus, Sulfur Silicon Relat. Elem.*, 2018, **193**(5), 273–279, DOI: 10.1080/10426507.2017.1399127.

36 O. S. Attarian, S. G. Matsoyan and S. S. Martirosyan, Synthesis of vinylpyrazoles, *Chem. Heterocycl. Compd.*, 2005, **41**(4), 533–536.

37 G. Serdaroğlu, N. Şahin, S. Şahin-Bölükbaşı and E. Üstün, Novel Ag (I)-NHC Complex: Synthesis, in Vitro Cytotoxic Activity, Molecular Docking, and Quantum Chemical Studies, *Z. Naturforsch., C: Biosci.*, 2022, **77**, 21–36, DOI: 10.1515/znc-2021-0130.

38 J. S. Moodley, S. B. N. Krishna, K. Pillay and P. Govender, Green Synthesis of Silver Nanoparticles from Moringa Oleifera Leaf Extracts and Its Antimicrobial Potential, *Adv. Nat. Sci. Nanosci. Nanotechnol.*, 2018, **9**(1), e015011, DOI: 10.1088/2043-6254/aaabb2.

39 M. J. Frisch, G. W. Trucks, H. B. Schlegel, G. E. Scuseria, M. A. Robb, J. R. Cheeseman, G. Scalmani, V. Barone, G. A. Petersson, H. Nakatsuji, X. Li, M. Caricato, A. V. Marenich, J. Bloino, B. G. Janesko, R. Gomperts, B. Mennucci, H. P. Hratchian, J. V. Ortiz, A. F. Izmaylov, J. L. Sonnenberg, D. Williams-Young, F. Ding, F. Lipparini, F. Egidi, J. Goings, B. Peng, A. Petrone, T. Henderson, D. Ranasinghe, V. G. Zakrzewski, J. Gao, N. Rega, G. Zheng, W. Liang, M. Hada, M. Ehara, K. Toyota, R. Fukuda, J. Hasegawa, M. Ishida, T. Nakajima, Y. Honda, O. Kitao, H. Nakai, T. Vreven, K. Throssell, J. A. Montgomery Jr, J. E. Peralta, F. Ogliaro, M. J. Bearpark, J. J. Heyd, E. N. Brothers, K. N. Kudin, V. N. Staroverov, T. A. Keith, R. Kobayashi, J. Normand, K. Raghavachari, A. P. Rendell, J. C. Burant, S. S. Iyengar, J. Tomasi, M. Cossi, J. M. Millam, M. Klene, C. Adamo, R. Cammi, J. W. Ochterski, R. L. Martin, K. Morokuma, O. Farkas, J. B. Foresman, and D. J. Fox, *Gaussian 16, Revision B.01*, Gaussian, Inc., Wallingford CT, 2016.

40 R. Dennington T. Keith and J. Millam, *Gaussview, Version 5*, Semichem Inc., Shawnee Mission, K. S, 2009.

41 S. G. Zhang, W. Lei, M. Z. Xia and F. Y. Wang, QSAR study on N-containing corrosion inhibitors: Quantum chemical approach assisted by topological index, *J. Mol. Struct. Teochem.*, 2005, **732**, 173–182, DOI: 10.1016/j.theochem.2005.02.091.

42 F. Sue Legge, G. L. Nyberg and J. B. Peel, DFT Calculation for Cu-, Ag-, and Au- Containing Molecules, *J. Phys. Chem. A*, 2001, **105**, 7905–7916, DOI: 10.1021/jp0101918.

43 S. M. Hiremath, A. Suvitha, N. R. Patil, C. S. Hiremath, S. S. Khemalapure, S. K. Pattanayak, V. S. Negalurmath and K. Obelannavar, Molecular Structure, Vibrational Spectra, NMR, UV, NBO, NLO, HOMO-LUMO and Molecular Docking of 2-(4, 6-Dimethyl-1-Benzofuran-3-Yl) Acetic Acid (2DBAA): Experimental and Theoretical Approach, *J. Mol. Struct.*, 2018, **1171**, 362–374, DOI: 10.1016/j.molstruc.2018.05.109.

44 E. G. Sağlam, E. Bulat, C. T. Zeyrek, H. Dal and T. Hökelek, Syntheses of and Structural Studies on Some Square Planar Dithiophosphonato Ni(II) Complexes, Octahedral Pyridine Derivatives Thereof and X-Ray Crystallography, DFT and Molecular Docking Studies of the Latter, *J. Mol. Struct.*, 2019, **1178**, 112–125, DOI: 10.1016/j.molstruc.2018.09.084.

45 Y. T. Hussein and Y. H. Azeez, DFT Analysis and in Silico Exploration of Drug-Likeness, Toxicity Prediction, Bioactivity Score, and Chemical Reactivity Properties of the Urolithins, *J. Biomol. Struct. Dyn.*, 2023, **41**(4), 1168–1177, DOI: 10.1080/07391102.2021.2017350.

46 A. Daina, O. Michielin and V. Zoete, SwissADME: a free web tool to evaluate pharmacokinetics, drug-likeness and medicinal chemistry friendliness of small molecules, *Sci. Rep.*, 2017, **7**, 42717, DOI: 10.1038/srep42717.

47 A. Daina, O. Michielin and V. Zoete, iLOGP: a simple, robust, and efficient description of *n*-octanol/water partition coefficient for drug design using the GB/SA approach, *J. Chem. Inf. Model.*, 2014, **54**(12), 3284–3301, DOI: 10.1021/ci500467k.

48 A. Daina and V. Zoete, A BOILED-Egg to predict gastrointestinal absorption and brain penetration of small molecules, *ChemMedChem*, 2016, **11**(11), 1117–1121, DOI: 10.1002/cmdc.201600182.

49 C. Wiles, P. Watts and S. J. Haswell, The application of micro reactor technology for the synthesis of 1,2-Azoles, *Org. Process Res. Dev.*, 2004, **8**, 28–32, DOI: 10.1021/op034125a.

50 B. Ren, M. Wang, J. Liu, J. Ge and H. Dong, Enhanced Basicity of Ag_2O by Coordination to Soft Anions, *ChemCatChem*, 2015, **7**(5), 761–765, DOI: 10.1002/cctc.201403035.

51 J. M. Hyes, M. Viciano, E. Peris, G. Ujaque and A. Ledos, Mechanism of Formation of Silver *N*-Heterocyclic Carbenes Using Silver Oxide: A Theoretical Study, *Organometallics*, 2007, **26**, 6170–6183, DOI: 10.1021/om700898d.

52 E. O. Karaca, E. Mızrak, N. Gürbüz, E. Çetinkaya, E. Karcı, M. Dündar, I. Ozdemir, A. Koç, I. Ozdemir, W. Koko, S. M. Al-Hazmy and M. Hamdi, Novel N-Heterocyclic Carbene Silver (I) Complexes: Synthesis, Structural Characterisation, Antimicrobial and Cytotoxicity Potential Studies, *Inorg. Chim. Acta*, 2025, **577**, e122458, DOI: 10.1016/j.ica.2024.122458.

53 N. Farah, H. Zin, S. Yee, S. Ooi, B. Khor, N. J. Chear, W. Kit, C. Siu, M. R. Razali, R. A. Haque and W. Yam, Cytotoxicity of Asymmetric Mononuclear Silver (I)-N-Heterocyclic Carbene Complexes against Human Cervical Cancer: Synthesis, Crystal Structure, DFT Calculations and Effect of Substituents, *J. Organomet. Chem.*, 2022, **976**, e122439, DOI: 10.1016/j.jorganchem.2022.122439.

54 H. Karci, M. Dündar, Z. Nawaz, İ. Özdemir, N. Gürbüz, A. Koç, İ. Özdemir, L. Mansour and N. Hamdi, Synthesis, Characterisation, Anticancer and Antimicrobial Activity of Ag-N-Heterocyclic Carbene Complexes Containing Benzimidazole Derivatives, *Inorg. Chim. Acta*, 2024, **565**, e121992, DOI: 10.1016/j.ica.2024.121992.

55 H. Ibrahim and M. D. Bala, Earth-abundant metal complexes of donor functionalised N- heterocyclic carbene ligands: synthesis, characterisation and application as amination catalysts, *New J. Chem.*, 2016, **40**(8), 6986–6997, DOI: 10.1039/C6NJ01118G.

56 H. Ibrahim and M. D. Bala, Improved Methods for the Synthesis and Isolation of Imidazolium Based Ionic Salts, *Tetrahedron Lett.*, 2014, **55**(46), 6351–6353, DOI: 10.1016/j.tetlet.2014.09.116.

57 R. Y. Nadeem, M. Yaqoob, W. Yam, R. A. Haque and N. A. Iqbal, Synthesis, Characterization and Biological

Evaluation of Bis -Benzimidazolium Salts and Their Silver (I)-N-Heterocyclic Carbene Complexes, *Med. Chem. Res.*, 2022, **31**, 1783–1791, DOI: 10.1007/s00044-022-02942-7.

58 S. Bera, G. G. Zhanel and F. Schweizer, Design, synthesis, and antibacterial activities of neomycin-lipid conjugates: polycationic lipids with potent Gram-positive activity, *J. Med. Chem.*, 2008, **51**(19), 6160–6164.

59 J. Zhang, K. Keller, J. Y. Takemoto, M. Bensaci, A. Litke, P. G. Czyryca and C. W. T. Chang, Synthesis and Combinational Antibacterial Study of 5″-Modified Neomycin, *J. Antibiot.*, 2009, **62**(10), 539–544, DOI: 10.1038/ja.2009.66.

60 Z. A. I. Alaridhee, M. Z. Ghadhyeb and H. J. Majeed, Synthesis and Biological Activity of New Silver Complexes with N-Heterocyclic Carbene Ligands, *Int. J. Health Sci.*, 2022, **6**, 7439–7447, DOI: 10.53730/ijhs.v6nS2.6865.

61 A. Sarfraz, R. Ashraf, S. Ali, T. Taskin-tok, Z. Khalid, S. Ullah, T. Kahlid, M. Mushtaq, S. M. El-bahy and Z. M. El-bahy, Synthesis, In Silico and in Vitro Studies of Silver (I)-N Heterocyclic Carbene Complexes, *J. Mol. Struct.*, 2022, **1251**, e131946, DOI: 10.1016/j.molstruc.2021.131946.

62 M. Donmez and M. Turkyilmaz, The New Pincer-Type NHCs Obtained by Synthesizing Ag(I)-NHC Complexes with Various Tails Containing Hydroxyl or Acetate Derivatives: Structural Properties and in Vitro Antibacterial Activities, *J. Mol. Liq.*, 2024, **415**, e126270, DOI: 10.1016/j.molliq.2024.126270.

63 G. Y. Xu, I. S. Zhao, C. Y. K. Lung, I. X. Yin, E. C. M. Lo and C. H. Chu, Silver Compounds for Caries Management, *Int. Dent. J.*, 2024, **74**(2), 179–186, DOI: 10.1016/j.identj.2023.10.013.

64 S. Medici, M. Peana, V. M. Nurchi and M. A. Zoroddu, Medical Uses of Silver: History, Myths, and Scientific Evidence, *J. Med. Chem.*, 2019, **62**, 5923–5943, DOI: 10.1021/acs.jmedchem.8b01439.

65 T. D. Tavares, J. C. Antunes, J. Padrão, A. I. Ribeiro, A. Zille, M. T. P. Amorim, F. Ferreira and H. P. Felgueiras, Activity of Specialized Biomolecules against Gram-Positive and Gram-Negative Bacteria, *Antibiotics*, 2020, **9**(6), 1–16, DOI: 10.3390/antibiotics9060314.

66 L. Ronga, M. Varcamonti and D. Tesauro, Structure-Activity Relationships in NHC-Silver Complexes as Antimicrobial Agents, *Molecules*, 2023, **28**(11), e4435, DOI: 10.3390/molecules28114435.

67 P. A. M. Guzman, W. van Schaik, M. R. Rogers, T. M. Coque, F. Baquero, J. Corander and R. J. L. Willems, Global Emergence and Dissemination of Enterococci as Nosocomial Pathogens: Attack of the Clones?, *Front. Microbiol.*, 2016, **7**, e788, DOI: 10.3389/fmicb.2016.00788.

68 J. Obszynski, H. Loidon, A. Blanc, J. M. Weibel and P. Pale, Targeted Modifications of Neomycin and Paromomycin: Towards Resistance-Free Antibiotics?, *Bioorg. Chem.*, 2022, **126**, e105824, DOI: 10.1016/j.bioorg.2022.105824.

69 D. Demir Atlı and D. Aksu, Air Stable N-Heterocyclic Carbene Silver Complexes: Synthesis, Characterisation, and Antibacterial Activity, *J. Coord. Chem.*, 2023, **76**(11–12), 1497–1506, DOI: 10.1080/00958972.2023.2251077.

70 U. Tutar and C. Celik, Antibiofilm and Antimicrobial Properties of 1-allyl-3-(2-diisopropylaminoethyl) Benzimidazolium Chloride and its Silver(I)-NHC Complex, *Cumhuriyet Sci. J.*, 2022, **43**(3), 432–436, DOI: 10.17776/csj.1121787.

71 R. Ruhal and R. Kataria, Biofilm Patterns in Gram-Positive and Gram-Negative Bacteria, *Microbiol. Res.*, 2021, **251**, e126829, DOI: 10.1016/j.micres.2021.126829.

72 S. Y. Hussaini, R. A. Haque, U. F. M. Haziz, A. A. Amirul and M. R. Razali, Dinuclear Silver (I)- and Gold (I)-N-Heterocyclic Carbene Complexes of N-Alkyl Substituted Bis-Benzimidazol-2-Ylidenes with Aliphatic Spacer: Synthesis, Characterizations and Antibacterial Studies, *J. Mol. Struct.*, 2021, **1246**, e131187, DOI: 10.1016/j.molstruc.2021.131187.

73 N. Ruwizhi, T. Singh, B. Omondi and M. D. Bala, Recent Developments in the Antimicrobial Efficacy of Coinage Metal (Cu, Ag, and Au) N-Heterocyclic Carbene Complexes, *ChemistrySelect*, 2025, **10**(14), e202500212, DOI: 10.1002/slct.202500212.

74 E. G. Sağlam, E. Bulat, C. T. Zeyrek, H. Dal and T. Hökelek, Syntheses of and Structural Studies on Some Square Planar Dithiophosphonato Ni(II) Complexes, Octahedral Pyridine Derivatives Thereof and X-Ray Crystallography, DFT and Molecular Docking Studies of the Latter, *J. Mol. Struct.*, 2019, **1178**, 112–125, DOI: 10.1016/j.molstruc.2018.09.084.

75 S. Noreen and S. H. Sumrra, Correlating the Charge Transfer Efficiency of Metallic Sulfa-Isatins to Design Efficient NLO Materials with Better Drug Designs, *BioMetals*, 2022, **35**(3), 519–548, DOI: 10.1007/s10534-022-00385-6.

76 A. M. Asiri, S. A. Khan, H. M. Marwani and K. Sharma, Synthesis, Spectroscopic and Physicochemical Investigations of Environmentally Benign Heterocyclic Schiff Base Derivatives as Antibacterial Agents on the Bases of in Vitro and Density Functional Theory, *J. Photochem. Photobiol., B*, 2013, **120**, 82–89, DOI: 10.1016/j.jphotobiol.2013.01.007.

77 M. Milusheva, M. Todorova, V. Gledacheva, I. Stefanova, M. Feizi-Dehnayebi, M. Pencheva, P. Nedialkov, Y. Tumbarski, V. Yanakieva, S. Tsoneva and S. Nikolova, Novel Anthranilic Acid Hybrids-An Alternative Weapon against Inflammatory Diseases, *Pharmaceuticals*, 2023, **16**(12), e16160, DOI: 10.3390/ph16121660.

78 M. Li, X. He, B. Wang, D. Zhao, C. Rong, P. K. Chattaraj and S. Liu, Changes in Structure and Reactivity of Ng2 Encapsulated in Fullerenes: A Density Functional Theory Study, *Front. Chem.*, 2020, **8**, 1–10, DOI: 10.3389/fchem.2020.00566.

79 E. Üstün, N. Özdemir and N. Şahin, Activity Analysis of New N-Heterocyclic Carbenes and Silver-Heterocyclic Carbene Molecules against Novel Coronavirus by UV-Vis, Fluorescence Spectroscopy and Molecular Docking, *J. Coord. Chem.*, 2022, **74**, 3109–3126, DOI: 10.1080/00958972.2022.2026935.

80 N. Ruwizhi, T. Singh, B. O. Omondi and M. D. Bala, Biological Activity of Late Transition Metal-Based Compounds: From Computational and Theoretical Studies

to Laboratory Exploration and Beyond, *Bioinorg. Chem. Appl.*, 2024, **2024**, e2829283, DOI: 10.1155/2024/2829283.

81 M. Wajid, M. Uzair, G. Muhammad, F. Siddique, A. Ashraf, S. Ahmad and A. F. Alasmari, Biological Activities, DFT and Molecular Docking Studies of Novel Schiff Bases Derived from Sulfamethoxypyridazine, *ChemistrySelect*, 2024, **9**(15), e202400675, DOI: 10.1002/slct.202400675.

82 Z. Akbari, C. Stagno, N. Iraci, T. Efferth, E. A. Omer, A. Piperno, M. Montazerozohori, M. Feizi-Dehnayebi and N. Micale, Biological Evaluation, DFT, MEP, HOMO-LUMO Analysis and Ensemble Docking Studies of Zn(II) Complexes of Bidentate and Tetradentate Schiff Base Ligands as Antileukemia Agents, *J. Mol. Struct.*, 2024, **1301**, e137400, DOI: 10.1016/j.molstruc.2023.137400.

83 B. S. Kusmariya, S. Tiwari, A. Tiwari, A. P. Mishra, G. A. Naikoo and U. J. Pandit, Theoretical and Experimental Studies of Two Co(II) and Ni(II) Coordination Complex with N,O Donor 2-Chloro-6-{[(4-Hydroxy-3-Methoxyphenyl)Methylidene]Amino}-4 Nitrophenol Ligand, *J. Mol. Struct.*, 2016, **1116**, 279–291, DOI: 10.1016/j.molstruc.2016.03.029.

84 S. Chatterjee, M. Afzal, P. C. Mandal, R. Modak, M. Guin and S. Konar, Exploration of Supramolecular Interactions, Hirshfeld Surface, FMO, Molecular Electrostatic Potential (MEP) Analyses of Pyrazole Based Zn(II) Complex, *J. Indian Chem. Soc.*, 2024, **101**(10), e101275, DOI: 10.1016/j.jics.2024.101275.

85 E. O. Akintemi, K. K. Govender and T. Singh, A DFT Study of the Chemical Reactivity Properties, Spectroscopy and Bioactivity Scores of Bioactive Flavonols, *Comput. Theor. Chem.*, 2022, **1210**, e113658, DOI: 10.1016/j.comptc.2022.113658.

86 S. Zinatloo-Ajabshir, S. Rakhshani, Z. Mehrabadi, M. Farsadrooh, M. Feizi-Dehnayebi, S. Rakhshani, M. Dušek, V. Eigner, S. Rtimi and T. M. Aminabhavi, Novel Rod-like $[Cu(Phen)_2(OAc)]\cdot PF_6$ Complex for High-Performance Visible-Light-Driven Photocatalytic Degradation of Hazardous Organic Dyes: DFT Approach, Hirshfeld and Fingerprint Plot Analysis, *J. Environ. Manage.*, 2024, **350**, e119545, DOI: 10.1016/j.jenvman.2023.119545.

87 E. Mohanapriya, S. Elangovan, N. Kanagathara, M. K. Marchewka, J. Janczak and P. Revathi, Density Functional Theory Calculations, Structural and Spectroscopic Characterization, and Solvent-Dependent HOMO-LUMO Studies of 2-Nitro-4-Methylanilinium Benzenesulfonate, *J. Mol. Struct.*, 2024, **1317**, e139147, DOI: 10.1016/j.molstruc.2024.139147.

88 S. Kondabanthini, N. K. Katari, M. Srimannarayana, R. Gundla, R. Kapavarapu and M. Pal, Wang Resin Catalyzed Sonochemical Synthesis of Dihydropyrano[2,3-c] Pyrazole Derivatives and Their Interactions with SIRT1, *J. Mol. Struct.*, 2022, **1266**, e133527, DOI: 10.1016/j.molstruc.2022.133527.

89 D. Shah, Ajazuddin and S. Bhattacharya, Role of Natural P-Gp Inhibitor in the Effective Delivery for Chemotherapeutic Agents, *J. Cancer Res. Clin. Oncol.*, 2023, **149**(1), 367–391, DOI: 10.1007/s00432-022-04387-2.